Determination of the local density of polydisperse nanoparticle assemblies

Anne-Caroline Genix, Julian Oberdisse

Determination of the local density of polydisperse nanoparticle assemblies

Anne-Caroline Genix* and Julian Oberdisse

Laboratoire Charles Coulomb (L2C), UMR 5221 CNRS, Université de Montpellier, F-34095 Montpellier, France

Revised manuscript

** Author for correspondence: anne-caroline.genix@umontpellier.fr*

ABSTRACT

Quantitative characterization of the average structure of dense nanoparticle assemblies and aggregates is a common problem in nanoscience. Small-angle scattering is a suitable technique, but it is usually limited to not too big assemblies due to the limited experimental range, low concentrations to avoid interactions, and monodispersity to keep calculations tractable. In the present paper, a straightforward analysis of the generally available scattered intensity – even for large assemblies, at high concentrations – is detailed, providing information on the local volume fraction of polydisperse particles with hard sphere interactions. It is based on the identical local structure of infinite homogeneous nanoparticle assemblies and their subsets forming finite-sized clusters. The approach is extended to polydispersity, using Monte-Carlo simulations of hard and moderately sticky hard spheres. As a result, a simple relationship between the observed structure factor minimum – termed the correlation hole – and the local volume fraction κ on the scale of neighboring particles is proposed and validated through independent aggregate simulations. The relationship shall be useful as an efficient tool for the structural analysis of arbitrary aggregated colloidal systems.

1. Introduction

Nanoparticle (NP) assemblies are formed under many different circumstances, for instance in suspensions due to lack of colloidal stability [1], in polymer matrices [2, 3], or upon drying of suspensions [4]. Some of these NP assemblies have important industrial applications, like e.g. reinforcing filler aggregates in car tires, [5] or the formation of porous membrane structures from NPs for electrocatalytical applications [6]. Knowing details of such structures allows understanding of transport properties related to connectivity, like conductivity [7], or mechanical reinforcement associated with force transmission [8]. Other studies pursue fundamental goals, like understanding the influence of physico-chemical properties of the environment on interparticle interactions governing NP assemblies. Such interactions may be temperature-dependent, as in hybrid functional polymer-NP systems aiming at a control of optical properties via aggregation, [9] or dominated by biologically relevant ions in systems mimicking NP assembly in cells [10]. Particular interactions may lead to specific aggregates, like the formation of NP chains which has been related to the combined presence of hydrogen bonding and dipolar interactions. [11] In polymer-composites, the effect of the polymer-mediated interactions, in particular via polymer grafts, on final aggregate structure has been investigated. [12, 13] On the other extreme, the dynamics of polymer surrounding well-dispersed NPs due to favorable polymer-particle interactions have attracted considerable interest. [14-16]

The structure of such assemblies is usually studied by electron microscopy [6, 11, 17, 18], or alternatively by scattering techniques [19, 20], in particular small-angle scattering suitable for NPs. Direct imaging techniques are attractive as they produce results which can be intuitively understood; unfortunately, they often suffer from limited representativity due to lack of statistics. Moreover, both sample preparation – like slicing for transmission electron microscopy (TEM) – and artefacts like particle superposition leading to miscounts may alter the results, even if impressive progress has been made with tomographic methods [21]. Note that some groups use the complementarity of scattering and electron microscopy to overcome the shortcomings of both methods. [13, 22-24]

On the other hand, scattering techniques are quite outstanding as they provide average information on three dimensional NP arrangements on the nanoscale. Well-dispersed NPs in solutions or polymer matrices have been analyzed by SAXS. [13, 25] When NPs assemble, the low-q intensity increases due to the growth of the zones containing NPs with correlated positions.[19] This low-q upturn may follow a power law [26], and then a fractal dimension can be extracted from the data with a power law fit, or literature expressions[26-29]. In some cases, in particular for small aggregates with scattering entering the experimentally accessible q-range completely, average aggregation numbers and radii of gyration can be determined directly. In this context, the unified law by Beaucage [27, 30] has been applied successfully, also for multi-level structures [31, 32]. Note that this is usually not possible for bigger assemblies, or interacting aggregates. In the case of sufficiently monodisperse NPs, crystallization

leads to the emergence of well-defined scattering peaks allowing the resolution of both local order – and thus distances and densities–, and average crystallite size [33]. Most NPs, however, are polydisperse in particle size (and sometimes shape, here we focus on spherical shapes), [34] polydispersity being typically in the range of 5 to 40%, depending on the synthesis protocol and the particle size. In practice, this leads to a large number of partial structure factors, which can sometimes be reduced by regrouping them (binning), but which are not easily measured independently, e.g., using deuteration or fluorination [35, 36]. In general, an experimental (sometimes called 'apparent') structure factor representing a weighted average of all partial structure factors is thus measured.

Since the pioneering calculations of D'Aguanno et al [37], it is well known that polydispersity makes the experimental structure factor peaks shrink until they possibly disappear completely. It is thus difficult to extract structural information from such low intensity signals. On the contrary, the depression of the structure factor at wave vectors just below the NP-NP interaction peak (or whatever remains of it) is a strong signature of the repulsive interactions between NPs. We call this low-q depression the correlation hole [38], in analogy with the excluded volume correlation hole in the direct-space pair correlation function, g(r). In particular, as already shown by D'Aguanno [37], polydispersity induces an increase of the low-q intensity. Rather involved theoretical integral-equation approaches based on solutions of the Ornstein-Zernike equation for polydisperse hard spheres (HS) and sticky hard spheres have been used, see also refs. [39-46] A similar method will be used as cross check in this article. [39-41] In the most complex cases, including both stickiness and polydispersity, equations have to be solved numerically [42]. Available analytical results will be used as a reference for our simulations, which are preferred here due to the homogeneity of a single-method approach, possibly uncontrolled analytical approximations as shown later in the text, a higher degree of freedom in the choice of the interactions, the availability of real-space representations, and the simplicity of the final formula proposed by us and applicable to scattering of any aggregate or particle assembly.

We have recently recognized the depth of the correlation hole as an experimental observable to follow the structure of filler aggregates in industrial [17, 22, 47] and model nanocomposites [23, 48]. In the present article, we have chosen a simulation approach to provide a universal tool for a large range of experiments: first, (log-normal) polydisperse hard sphere particles are created, and both "infinite" and finite NP assemblies representing aggregates of known particle density generated. Then, all partial interaction terms are summed, and the experimental structure factor is determined. The correlation hole at scattering wave vector q = 0 for "infinite" assemblies, and at finite q for aggregates is then mapped onto the local density. Finally, this mapping is explicitly shown to allow the determination of the local particle volume fraction in independently generated aggregates without further numerical work.

2. Simulation method and scattering analysis

Simulation details: configurations of systems of polydisperse spherical particles with hard sphere interactions are explored by randomly placing N = 8000 particles in a cubic simulation box of dimension L_{box}, with periodic boundary conditions, followed by an equilibration procedure of random displacements. The absence of finite-size effects has been checked and an example is shown in the ESI. The particles obey a log-normal size distribution function with parameters R_0 and σ, see [49], the latter polydispersity parameter being varied between 0 and 45% in this article, while R_0 is arbitrarily fixed to 10 nm in order to obtain scattering functions directly in the wave vector range usually probed by small-angle scattering from experimental NP systems. The only remaining parameter is the *global* volume fraction κ of the system defined by the ratio of total NP and box volume. For homogeneous systems, the global volume fraction is identical to the average *local* one (also termed 'compacity' in previous work) associated with the environment of individual particles on the scale of nearest neighbors, where the average is performed over all particles. The determination of κ from the scattering function is the objective of this article. In practice, high volume fractions are created by starting with smaller particle sizes giving lower volume fractions, and increasing the particle sizes progressively to their nominal values, during equilibration. Note that we work at a fixed number of particles, which implies that the box size L_{box} decreases for higher volume fractions. This is reflected by changes in $q_{min} = 2\pi/L_{box}$. After equilibration, structure factors (see below) representative of "infinite" systems are determined as averages over different configurations of the entire box, generating typically 50-100 independent systems, each being first equilibrated, and then 100 statistically independent structure factors are calculated by letting the system evolve in time – typically 100 steps per particle between each S(q). By performing multiple calculations, we have checked that the accuracy of this averaging procedure for S(q) is of the order of 1%. For finite-sized aggregates of know density (identical to the global one), an equivalent number of spherical subsets of N_{agg} particles is cut out of the central region of the equilibrated and evolving systems.

The study of local correlations between moderately sticky hard spheres at a fixed global volume fraction κ was done following a geometrical rather than thermodynamic approach of Baxter [50] or Gazzillo [42, 43], in order to maintain system homogeneity. Simulations are restrained to moderate stickiness because our mapping procedure is based on the equality of global and local volume fractions, which is only true for systems which are not destabilized by attractive interactions yielding phase separation. NP configurations (N = 8000) in a simulation box were first generated and equilibrated with only hard sphere interactions, as before. Then, spheres were made sticky, and each particle continues moving until hitting another one, i.e., a center-to-center distance equal to the sum of the radii. These two particles form a (heavier) group, which was considered immobile in order to avoid the collapse of the system and thus preserve homogeneity. Such groups conserve stickiness and can

grow further via subsequent collisions with free particles. The procedure was repeated until a majority of 80% of all NPs was stuck onto others, leaving thus a small part individually dispersed.

Determination of small-angle scattering: Structure factors are calculated differently for the entire simulation box representing an "infinite" system, and finite subsets. By treating the entire simulation box as the unit cell of an infinite cubic lattice, finite-size effects are avoided: the structure factor of the "infinite" system can be calculated at the reciprocal lattice points of the box, i.e., at certain q-values q_p defined below, and in certain directions compatible with the cubic lattice: [51-55]

$$S_{mono}(q_p) = \left|\sum_{j=1}^{N} \exp\left[-ip2\pi \frac{hx_j+ky_j+lz_j}{L_{box}}\right]\right|^2 \quad (1)$$

where the N (monodisperse) particles are located at positions (x_j,y_j,z_j), and the norm of the scattering vector is given by $q_p = p\, 2\pi \frac{\sqrt{h^2+k^2+l^2}}{L_{box}}$, with p = 1, 2, 3… . In practice, thirteen directions provide a good average, chosen as Miller indices 100, 110, and 111, and their respective equivalents. This leads to three series of q_p, obtained by multiplication of the first one with √2 and √3, which can then be unified in a single function. For polydisperse systems, each particle j is described by the Fourier transform of its scattering length density Δρ, which is called the form factor amplitude. Its prefactors are Δρ and the particle volume V_j, and the function normalized to 1 at low q is termed $F_j(q)$. The square of the non-normalized function (including the volume V_j) is commonly called the form factor $P_j(q)$, and it can be averaged over all particles, giving $\bar{P}(q)$. It is straightforward to include polydispersity in the above formalism, eqn (1), by weighting the exponential by the form factor:

$$I(q_p) = \left|\sum_{j=1}^{N} \Delta\rho\, F_j(q_p) V_j \exp\left[-ip2\pi \frac{hx_j+ky_j+lz_j}{L_{box}}\right]\right|^2 \quad (2a)$$

$$S(q_p) = \frac{I(q_p)}{\bar{P}(q_p)} \quad (2b)$$

where the experimental structure factor $S(q_p)$ with its apparent isothermal compressibility is obtained by dividing by the average form factor $\bar{P}(q)$ in eqn (2b), as done for finite assemblies below. Configurational averages are then performed on $S(q_p)$, simply written S(q) in what follows.

For finite-size assemblies of N_{agg} monodisperse particles, the structure factor can be calculated more efficiently using directly the isotropic average. For identical spherically symmetric nanoparticles, S(q) is the Fourier transform of the pair-correlation function of the center-of-mass positions of NPs. Using the Debye formula [56], it reads:

$$S(q) = 1 + \frac{2}{N}\sum_{i>j}^{N} \frac{\sin\left(q(r_j-r_i)\right)}{q(r_j-r_I)} = 1 + \frac{2}{N}\sum_{i>j}^{N} S_{ij}(q) \quad (3)$$

where (r_i - r_j) represents the distance between the centers-of-mass of NPs i and j, and the sinus term is regrouped in S_{ij} expressing the phase difference of waves scattered by particles i and j, its thermodynamic average over all particles of the same sizes being the partial structure factor. The low-q upturn of S(q) contains valuable information on the number of particles, and the spatial extent of the NP assembly. At large q, the interparticle correlation peak is usually found, and just below this q-value, the correlation hole. As with eqn (2b), the isotropically averaged intensity, i.e., the differential scattering cross section per unit sample volume I(q) can be calculated by the product of the monodisperse NP form factor, $P(q) = \Delta\rho^2\, V^2\, F^2(q)$, and the interparticle structure factor, S(q). [52]

Adding *polydispersity in size* for the spherical NPs requires to weight properly each contribution to the structure factor S_{ij} by its form factor ~~amplitude $F_j(q)$~~. The total scattered intensity is given by a weighted average [22], and one can again calculate the experimental structure factor by dividing by the average form factor:

$$S(q) = \frac{\sum_{i,j} V_i V_j\, F_i(q) F_j(q) S_{ij}(q)}{\sum_i V_i^2\, F_i^2(q)} \tag{4}$$

Analysis of small-angle scattering and mapping procedure: It is proposed to extract the local particle volume fraction κ through the following simple mapping procedure. First, the local volume fraction κ experienced by particles in an aggregate (or any other assembly) is determined by comparing its correlation hole structure factor to the low-q limit of S(q) of a "infinite" homogeneous HS fluid of known κ. A straightforward development of the PY equation at low q [57-59] or equivalently the Carnahan-Starling equation [60] gives the following limit for monodisperse particles setting α to one:

$$S_{PY}(q \to 0) = \frac{(1 - \alpha\,\kappa)^4}{(1 + 2\,\alpha\,\kappa)^2} \tag{5}$$

This limit is associated with the isothermal compressibility of the nanoparticle assembly. In eqn (5), we have introduced the empirical parameter α to allow a generalization to the description of polydisperse spheres, to be given in the results section. As a reference, we use the calculation by Vrij [46] for log-normal polydisperse HS. Using our symbols, it reads:

$$S_{PolyHS}(\kappa, \sigma) = (1-\kappa)^2 \left(1 - \frac{6\kappa}{1+2\kappa} \exp(-2\sigma^2) + \frac{9\kappa^2}{(1+2\kappa)^2} \exp(-3\sigma^2)\right) \tag{6}$$

In a second time, finite spherical assemblies of spheres are cut out of the homogeneous HS fluid. By construction, they have the same κ as the original system, a feature which is difficult to achieve with arbitrary aggregates or assemblies. Note that such spherical subsets have the lowest surface area, limiting thereby modifications of the signal by particles sitting close to the surface, and thus

experiencing locally lower densities. Using eqn (4), the structure factor now resembles finite-sized aggregates: it displays a low-q upturn, and a correlation hole, which can then be mapped onto an experimental one to determine the corresponding average density.

3. Results

The reference case of "Infinite" NP assemblies: We have undertaken numerical simulations of hard sphere NP assemblies in order to check the influence of concentration and polydispersity. The structure factor is calculated using eqn (1) and its generalization to polydispersity with eqns (2), and results are shown in Fig. 1. For monodisperse systems, one may note that it is numerically more efficient to Fourier transform the pair correlation function. As one can see in the inset of Fig. 1a, the result for monodisperse hard spheres is indistinguishable from the Percus-Yevick (PY) result [57], down to low q, in spite of the finite box size, for volume fractions ranging from 10 to 30%. Important features of S(q) of infinite assemblies of monodisperse spheres are (i) the low-q limit S(q→0) describing the isothermal compressibility, (ii) the high-q limit of one, and (iii) the position of the NP-NP correlation peak around π/R, R being the NP radius. Note that the first point (i) expressing a relationship between concentration and low-q scattering is the basis of the method proposed here. In Fig. 1a, the simulated structure factors are plotted as a function of polydispersity σ for a volume fraction κ of 20%, others are shown in the ESI.

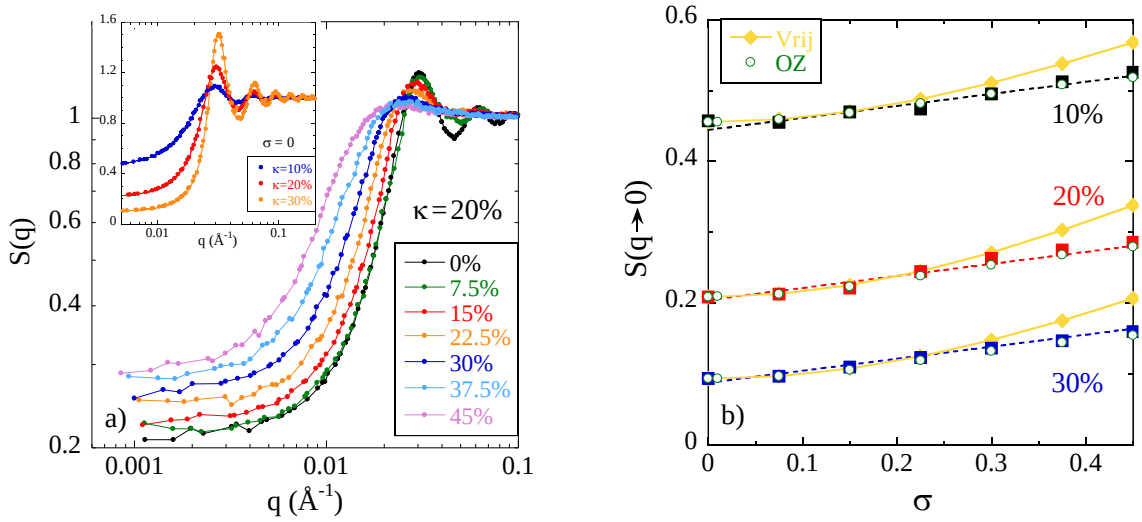

Fig. 1 (a) Log-log plot of the structure factor S(q) as a function of wave vector q for an "infinite" HS ensemble (R_0 = 10 nm, volume fraction 20%v), with polydispersity σ ranging from 0 to 45% as given in the legend. Inset: comparison of simulated structure factor for monodisperse (σ = 0) hard spheres with their analytical counterpart (lines, see text for details), for κ = 10, 20, and 30%. **(b)** Low-q limit S(q→0) as a function of polydispersity σ at different volume fractions κ, compared to calculations by Vrij [46] and numerical solutions of Ornstein-Zernike (OZ) [39, 40], see text for details. Solid lines are linear fits of common slope.

The structure factors in Fig. 1a at fixed volume fraction of $\kappa = 20\%$ highlight the following features: first, the structure factor peak around 0.03 $Å^{-1}$ is clearly due to NP correlations in contact, as $q_{peak} \approx \pi/R$. Secondly, the correlation hole is well defined even when the peak vanishes. The low-q values $S(q\rightarrow 0)$ are seen to increase with increasing polydispersity at low q, with consequences extending also towards the intermediate q-range. It is thus important to know the particle polydispersity if one wishes to determine aggregate densities from the low-q depression.

In Fig. 1b, we have regrouped all our results for $S(q\rightarrow 0)$ of "infinite" HS assemblies. As observed in Fig. 1a, $S(q\rightarrow 0)$ increases with polydispersity, and this increase is found to be linear, with a slope independent of κ. Naturally, the low-q limit decreases with the density κ, as illustrated in the inset of Fig. 1. The comparison with the reference calculation by Vrij, eqn (6), [46] is also shown in Fig. 1b. It illustrates two points: First, our simulations agree nicely with the predictions by Vrij for low and moderate polydispersities. Above some 30%, however, the Vrij-function shows an upward curvature. While there is no a priori reason why our simulation code should break down for higher polydispersities, in particular at low concentrations, we compared both predictions to an independent calculation based on the simultaneous numerical solution of Ornstein-Zernike integral equations for quasi-continuous size distribution. [39-41] The perfect superposition with our simulation results suggests that the latter are trustworthy, while some necessary approximations in the analytical model [46] induce the observed deviations at high polydispersities.

In order to finalize this part on the low-q scattering of HS assemblies, one can analyze vertical cuts in Fig. 1b, for each polydispersity. Examples for monodisperse and polydisperse ($\sigma = 15\%$ and 30%) HS particles are shown in Fig. 2. The fits were made using eqn (5), with the α_∞-parameters for these "infinite" systems given in the caption. The quality of the fits is very good. For monodisperse particles, the original Percus-Yevick result ($\alpha_\infty = 1$) is found; then α_∞ decreases with polydispersity, which corresponds to the increase in $S(q\rightarrow 0)$ described in Fig. 1a.

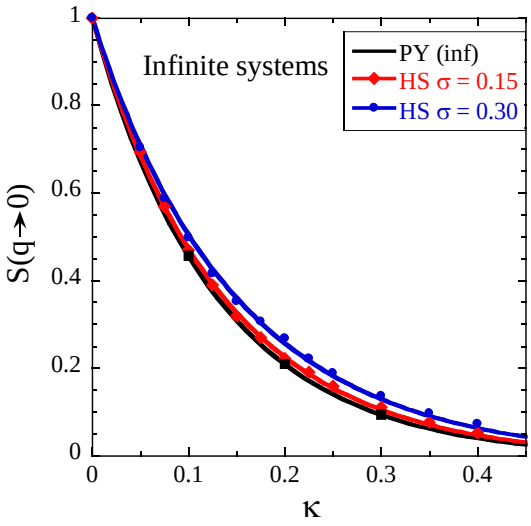

Fig. 2 Low-q structure factor S(q→0) of "infinite" system as a function of volume fraction based on simulations of hard spheres (polydispersity σ = 0, 15%, 30%). Solid lines are fits using eqn (4) with α_∞ = 1 (PY), 0.95, and 0.87, for σ = 0, 15, and 30%, respectively.

The description given in Fig. 2 can be performed for all polydispersities, and the result for α is well described by a parabolic function (shown later in the text):

$$\alpha_\infty(\sigma) = 1 - 1.13\,\sigma^2 \qquad (7)$$

It is thus possible to predict the outcome S(q→0) of our simulations for any particle polydispersity (below 45%) using eqns (5) and (7), and determine κ of any NP assembly by comparing to the corresponding correlation hole data. The parabolic shape is related to the observation in Fig. 2 showing that at first, with low polydispersity (σ from 0 to 15%), there is only little change. At higher σ, however, polydispersity becomes important.

One can also conclude on the accuracy of this κ–determination, in particular if the polydispersity is not exactly known. For an experimentally measured S(q→0) of 0.2, the uncertainty in volume fraction κ is typically from 22±1.5%, if the polydispersity ranges between 0 and 30%; even for S(q→0) = 0.1, the range in kappa is still rather reduced, 31.5±2.5%. This seems an acceptable error given the simplicity of the method. Interestingly, the shape of the curves in Fig. 3 makes the relative range of κ approximately constant, ca. 15%. One may thus conclude that the determination of the local density of the NPs arrangements is rather robust.

Two additional points may deserve discussion. First, while the decrease in S(q→0) observed in Fig. 2 is clearly related to the increase in local density, it is unclear how this translates to finite-sized aggregates. Secondly, real aggregates are formed by attractive interactions, and it is unclear how these affect the local correlations. Both points are addressed in the next sections.

Finite-sized NP assemblies of known density: Spherical assemblies of hard spheres of known average density κ have been generated by equilibrating an "infinite" HS system with periodic boundary conditions, and cutting out a spherical domain in the center of the simulation box, of radius such that the number of selected spheres equals N_{agg}. This is illustrated in Fig. 3. For practical reasons, it is sufficient to equilibrate HS assemblies with less than N = 8000 particles; most of what follows has been run with N = 2000, and N_{agg} = 200 central particles were selected. The advantage of this method is that the local density of the spherical aggregate equals the nominal one of the cubic simulation box. Note that it is sufficient to study individual spherical aggregates, as our analysis will be focused on intermediate-q vectors, which will be unaffected by interactions between aggregates at higher concentrations. Statistical averages are achieved as before, by letting the entire simulation box equilibrate and evolve before calculating structure factors.

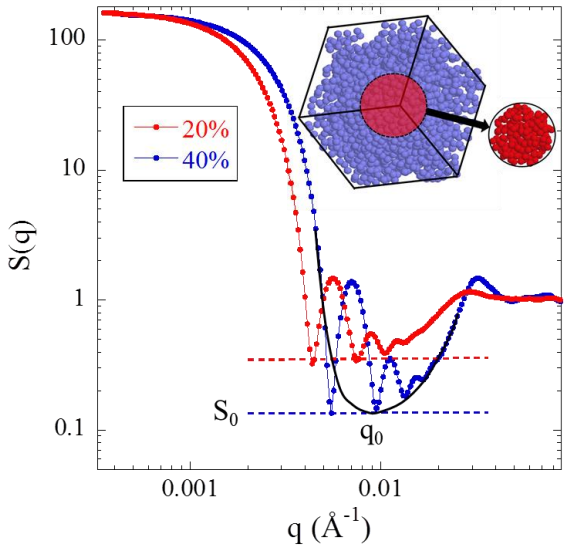

Fig. 3 Structure factor S(q) of finite spherical HS systems, for two volume fractions, κ = 20 and 40% (σ = 15%). q_0 represents the position of the correlation hole, the continuous black line illustrates its average shape. Inset: "Infinite" simulation box with equilibrated HS, and illustration of cutting out a finite spherical aggregate in the box center.

The structure factors are calculated using eqn (4), and examples are shown in Fig. 3 for two different densities. Their low-q value is essentially given by N_{agg}, with a small correction due to particle polydispersity, $\exp(-9\sigma^2)$, calculated using eqn (4). The low-q decrease is first due to a Guinier regime of finite-sized objects, and one sees that the assembly with higher concentration is smaller (N_{agg} being fixed), and decreases thus less rapidly. Due to the rather accurate definition of the spherical surface by the particles as illustrated in the inset, the symmetry of the object is high, and the spherical form-factor oscillations around q = 0.005 $Å^{-1}$ are thus quite pronounced. At high q, finally, an interparticle correlation peak is reached, with a position which is further to the right for the denser system, as expected. In between the form factor oscillations and the correlation peak, the structure factor is

depressed. The depth of this correlation hole decreases with the density, offering us the possibility to map its depth on the density, as done with infinite particle assemblies in the previous section. Its position extends over a limited q-range, but it is difficult to locate it exactly due to the multiple maxima and minima. We have drawn a continuous black line as guide to the eye describing the average shape of the correlation hole in Fig. 3. A good compromise for the position of its minimum between the vanishing low-q oscillations and the increase to the correlation peak appears to be the second local minimum starting from low-q, at q_0, and of value S_0. By performing calculations with different geometries (sphere, cubes, short cylinders, see ESI), we have checked that S_0 given by this second local minimum is robust. While the exact value of S_0 is affected by the geometry, it is mainly controlled by the local particle density, and it will be shown below that the choice of the sphere allows determining the density of aggregates of arbitrary shapes. Comparisons to fuzzy aggregate structures in the discussion will show the suitability of this estimation.

The next step is to generalize the example given in Fig. 3, and determine the structure factor at the correlation hole, S_0, as a function of κ, for different polydispersities, in analogy with Fig. 1 for "infinite" systems. In Fig. 4a, S_0 is plotted for volume fractions from 5 to 40%, for the moment at fixed NP polydispersity of 0, 15% and 30%. One immediately sees that these functions are well above the PY limit of infinite fluids, which demonstrates that the correlation hole of the "infinite" system only gives a first approximation for the one of finite-sized aggregates or assemblies. Note that our data are perfectly reproducible: to illustrate this, the κ = 12.5% (σ = 30%) concentration has been run twice, and the two points overlap in Fig. 4a. As in Fig. 2, the influence of polydispersity is to increase S_0, at first moderately, and quite markedly for σ = 30%. The fits with eqn (5) are superimposed to the data points in Fig. 4a. The quality of the fit is acceptable, with deviations showing up high concentrations, above 30%. The corresponding α-values (termed α_{finite}) are reported in the caption. These values are lower than the ones for "infinite" systems, translating the fact that the S_0-values are higher than the $S(q\rightarrow0)$ of the latter.

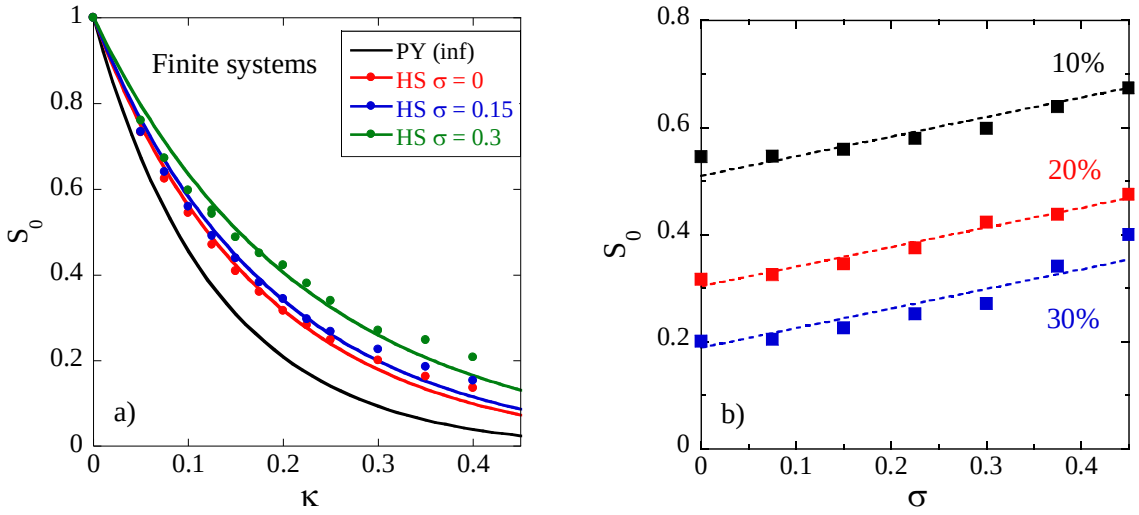

Fig. 4 (a) Low-q structure factor S_0 of finite (spherical) system as a function of volume fraction κ based on simulations of hard spheres (polydispersity σ = 0, 15, 30%). Solid lines are fits using eqn (5) with α_{finite} = 0.73, 0.69, and 0.57, for σ = 0, 15, and 30%, respectively. The black line is the (infinite) PY prediction. **(b)** S_0 as a function of σ for κ = 10, 20, and 30% (finite systems), respectively. Dotted lines are linear fits of common slope.

The plot of S_0 as a function of polydispersity (for different κ) is shown in Fig. 4b. As in Fig. 1b, the functional dependence on σ is found to be linear, with a slope independent of κ. However, the slope is higher than for the "infinite" system. We think that this is related to the different q-range under scrutiny: for infinite systems, we focus on q→0, whereas the finite ones have a correlation hole at finite q. Unlike at very low q, the structure factor in the latter range is more strongly affected by changes in local correlation, as we will see in the discussion section below. By fitting eqn (5) at fixed σ, the α_{finite}-parameters can be determined, and the result is plotted in Fig. 5a. Moreover, these data are compared to those of "infinite" systems described by eqn (7) in the same figure.

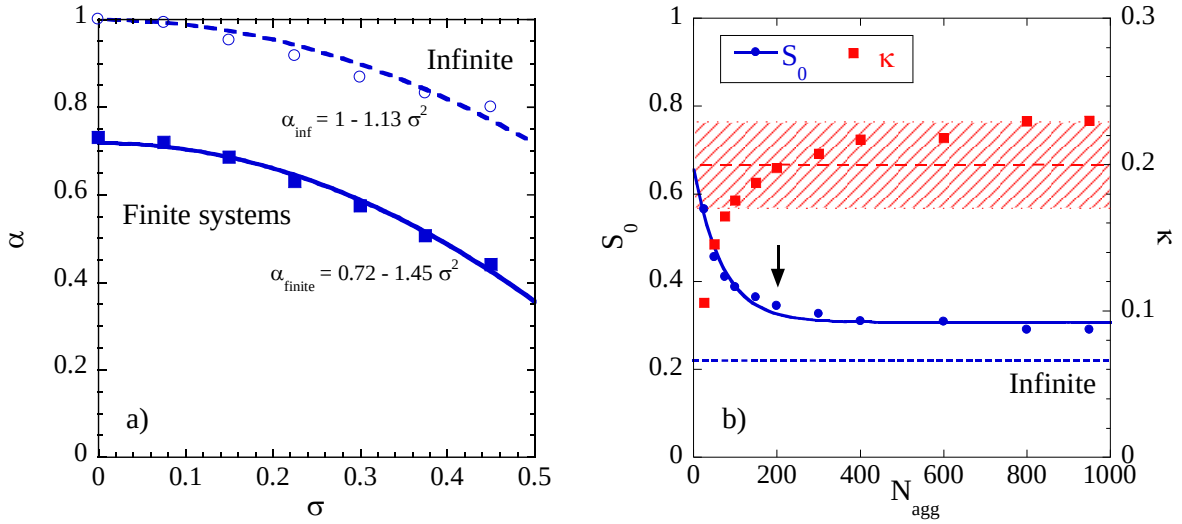

Fig. 5 (a) Evolution of fitted α_{finite}-parameter, as a function of polydispersity σ, for both "infinite" and finite systems. The lines are fits as given in eqns (7,8). **(b)** Left axis: correlation hole S_0 of κ = 20% (σ = 15%) spherical subsets as a function of N_{agg} of subset. The infinite limit for S_0 is also shown (broken line). Right: κ deduced from S_0, compared to dotted horizontal lines illustrating ±15% error.

α_{finite} is also a decreasing parabolic function, with a remarkably similar curvature, but shifted vertically to lower α. The result for $\alpha_{finite}(\sigma)$ reads:

$$\alpha_{finite}(\sigma) = 0.72 - 1.45\ \sigma^2 \qquad (8)$$

With eqn (8), it is possible to determine α for finite HS systems with any log-normal polydispersity σ between 0 and ca. 45%, and then employ eqn (5) to extract the local compacity κ from the experimental scattering data without further numerical work. The combination of eqns (5) and (8) thus represents the main result of this article. One may note that the values reported in Fig. 5a deviate from our results for HS-systems used in a preliminary calculation, [22] but remain remarkably close (α = 0.72 for σ = 15%), due to a compensation of two effects, the removal of the finite-size box effect obtained using eqn (1), and generation of finite assemblies.

We have shown in Fig. 5a how the effect of local volume fraction on the experimental isothermal compressibility of "infinite" systems S(q→0) translates into an effect on the correlation hole S_0 located at finite q-values for finite-sized aggregates characterized by a number of particles N_{agg}. Naturally, the choice of N_{agg} may be questioned. We have performed simulations with N_{agg} ranging from 25 to 1000 (adapting N for big assemblies, see ESI), and found that the representative depth of the correlation hole as taken at the 2nd S(q) minimum is robust. The result for κ = 20% (σ = 15%) is shown in Fig. 5b, where S_0 is plotted as a function of N_{agg}. S_0 is seen to tend to a plateau for large N_{agg}, whereas at low N_{agg} the spherical subsets are so small that they have a comparatively high surface area. Particles located at this surface have neighbors only on one side, thereby decreasing the effective local volume fraction. This induces an increase of S_0 towards one. The plateau value indicates also that

polydispersity in aggregate size would lead to an average lying on the same level. One can now calculate the κ one would obtain from this S_0, using eqns (5) and (8), and its value is superimposed to the plot. The nominal κ of 20% is found for aggregates having $N_{agg} \geq 100$, within a ±15% error interval illustrated by dotted lines. Finally, S(q→0) of the "infinite" calculation is also shown as a broken horizontal line. One would expect S_0 to tend more quickly towards S(q→0), but one should keep in mind that even 1000 particles correspond to only 10 particles along one direction, and which is too small to separate the length scales. This illustrates again that necessity of describing finite-sized systems.

Up to here, we have worked only with assemblies of hard spheres, which might be incompatible with a description of local interactions in, e.g. aggregates made by attractive (sticky) interactions. Our initial working hypothesis was that at high enough concentrations, above a threshold to be defined, the local environment is so crowded that even in absence of stickiness, neighbors are necessarily very close. In the next section, we will first check the validity of this hypothesis by comparing HS to mildly sticky particles, and then evaluate the predictions of our mapping procedure for rigid aggregates as they may be formed by inorganic NPs.

4. Discussion

The local correlations between NPs depend obviously on their interactions. We have therefore changed the type of interactions from purely hard sphere to mildly attractive, in order to explore the consequences on the depth of the correlation hole. As our mapping procedure relies on the generation of spatially uniform assemblies of spheres being described by a single volume fraction κ, strongly attractive NP systems leading to local phase separations are not suitable here. We have therefore designed the numerical procedure outlined in section 2 in order to produce globally homogeneous systems with locally sticky HS interactions. In Fig. 6a, the experimental structure factors for polydisperse spheres (σ = 15%) of hard and sticky hard spheres are compared at κ = 20%. At the bottom, the S(q) of "infinite" systems are superimposed. As one turns on the sticky interaction, the NP interaction peak moves to the right, but the low-q limit remains essentially unchanged. We interpret this as the confirmation of the global homogeneity in spite of the stickiness. At intermediate q, however, the structure factor of sticky beads shows a slower descent from the peak to the low-q limit, i.e. a higher signal. Together with the peak shift, this is thus the signature of the stickiness as generated here. This is also the q-region where polydispersity affects local correlations more strongly, as discussed in section 3. For comparison with the finite NP assemblies, their S(q) are shifted vertically in Fig. 6a. They display exactly the same features, from HS to sticky: unchanged low-q behavior, a slight increase at intermediate q, and a shift of the correlation peak. By comparing the depth of the

correlation hole, it can be concluded that the structure factor at q_0 as defined in Fig. 3 is moderately increased due to stickiness.

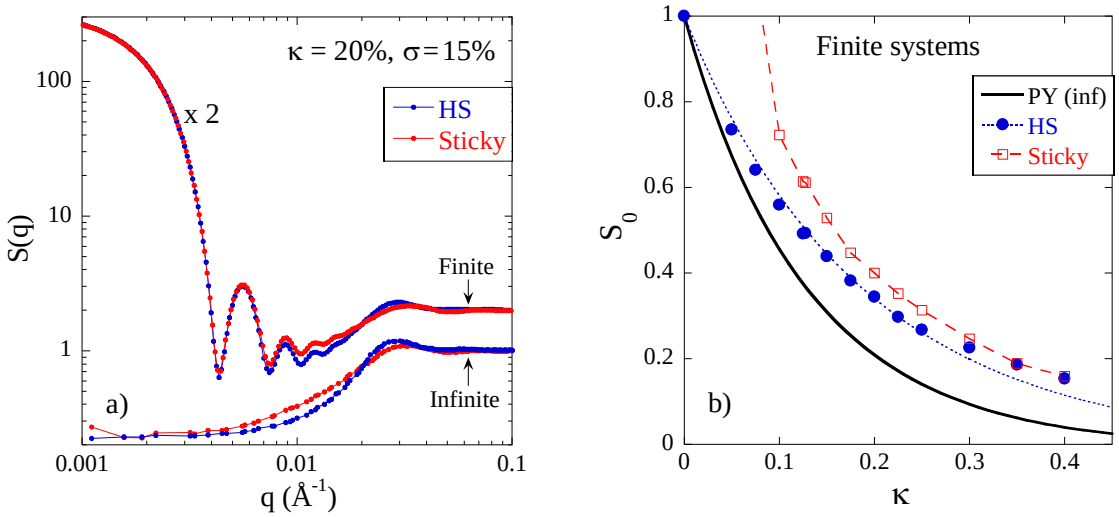

Fig. 6 (a) Comparison of sticky to hard sphere structure factor, for "infinite" and finite (multiplied by 2 for clarity) systems (κ = 20%, σ = 15%). **(b)** Comparison of sticky to hard sphere structure factor minimum S_0 as a function of κ (σ = 15%).

The structure factor at the correlation hole S_0 is plotted as a function of κ in Fig. 6b, for finite systems, for both hard and sticky hard spheres with σ = 15%. The two curves deviate at low volume fractions. The strong increase of the S_0 of the sticky system is probably related to the generation of spatial heterogeneities caused by strong density fluctuations possible at low κ. S_0 then exceeds 1 as illustrated by the strongly increasing dotted line. At high enough densities, the structure factor S_0 of the sticky system progressively approaches the HS one. This confirms our initial hypothesis that at high κ, the interaction is dominated by the infinite hard sphere potential, and the system designed to be only moderately sticky is indeed preserved from large-scale heterogeneity. As in section 3, one can estimate the error made by using the HS formalism instead of stickiness by visual inspection of Fig. 6b, and a few percents error on κ are found as long as κ is high enough, say above some 10%. Alternatively, one could parametrize S_0 of the sticky interactions, and would obtain estimations even in this low local density range.

Finally, the performance of the combination of eqns (5) and (8) must be evaluated, in particular for "real" aggregates composed of chemically bound particles, as encountered in typical experimental situations [18]. We therefore apply our mapping procedure to simulated aggregates made of polydisperse NPs mimicking real aggregates. This is a severe test of the hypothesis of dominant hard sphere interactions, as all NPs are glued together irreversibly, without any dynamics, whereas eqns (5,8) are based on simulations subsets of homogeneous hard sphere assemblies. Different construction algorithms based on ref. [18] have been developed in order to produce aggregates of different structure

and density, and are outlined in the ESI. We start with the discussion of rather open aggregates. In Fig. 7a the intensity I(q) averaged over several hundred aggregates, the average NP form factor rescaled to the same contrast and concentration, and the average structure factor are plotted, together with a graphical representation of one aggregate (N_{agg} = 200, R_0 = 10 nm, σ = 15%), which appears to be rather fuzzy. Note that there is no control of coordination numbers with this type of construction. S(q) has the properties and the typical shape described above: a low-q upturn due to aggregation followed by a short, possibly fractal regime (d_f compatible with 1.5), a contribution below one (correlation hole at q_0) due to NP repulsion in the intermediate-q range, and a peak related to the interparticle distance. This peak is not very prominent due to polydispersity, whereas the correlation hole remains well-defined.

For comparison, the explicit calculation of the experimental structure factor of a finite hard sphere system of the same size distribution (R_0 = 10 nm, σ = 15%) for κ = 11.5% is also superimposed to the aggregate structure factor in Fig. 7a, where the choice of 11.5% is discussed below. Obviously, the shape is not the same, as it is spherical by definition of the subset, whereas the aggregate is fuzzy: the low-q domain thus differs. In the high-q range, the exact position of the structure factor peak is not reproduced either, as spheres move around some average distance in the hard sphere system, and are not stuck to each other as in the aggregate. Neither of these two features is relevant for the present discussion, which focuses on the average depth of the correlation hole, well reproduced in Fig. 7a.

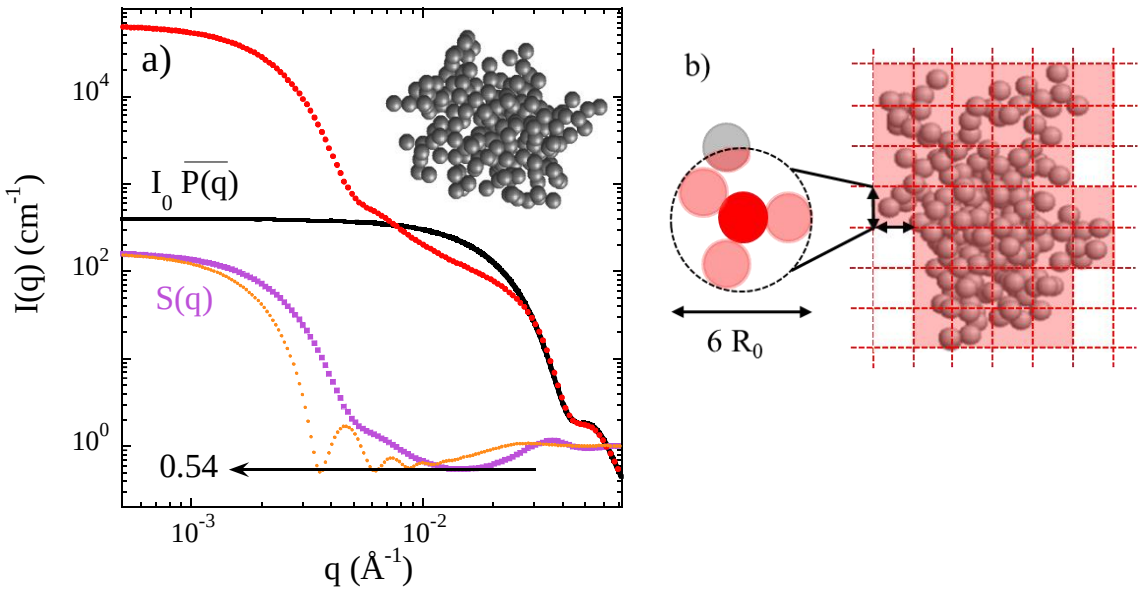

Fig. 7 (a) Example of average I(q), the average particle form factor $\overline{P(q)}$, and the resulting S(q) as a function of wave vector q of simulated aggregates of N_{agg} = 200 polydisperse NPs (R_0 = 10 nm, σ = 15%). S(q) is compared to the simulated structure factor of a finite HS system at 11.5% (orange symbols, same parameters). In the inset, a 3D snapshot of one aggregate is shown (polydispersity is not graphically represented). **(b)** Determination of aggregate volume by discretizing on the scale of the first coordination shell.

The aim of the mapping procedure is to estimate the local volume fraction within the aggregate. Reading off $S_0 = 0.54$ from Fig. 7a, an average local volume fraction felt by the NPs in the aggregate of $\kappa = 11.5\%$ is determined using $\alpha_{finite}(\sigma) = 0.72 - 1.45\ \sigma^2 = 0.69$. For comparison, one may estimate the total volume fraction of aggregates like the one shown in Fig. 7a from their total particle volume and the global size given by the circumscribing sphere: one finds an average for κ of about 7.5%. Due to the presence of voids within the aggregate, this must be a lower bound for κ describing local interactions between particles, and a more appropriate method to estimate κ needs to be developed. As illustrated in Fig. 7b, the aggregate volume can be better estimated by discretizing the total volume into small cubes. One may then count the number of cubes being occupied by at least one particle, and estimate the corresponding compacity κ_{agg} from the ratio of the known particle volume, and the aggregate volume. The choice of the cube size is crucial, as one wishes to follow local density fluctuations on the scale of $1/q_0$. The position q_0 of the correlation hole being closely related to the correlation peak of particles in contact, the first coordination shell is a suitable candidate for the cube size: it is chosen such that the cube contains the coordination shell, i.e. its linear size is $6R_0$, see Fig. 7b. Much bigger cubes would include local voids, whereas too small ones would simply identify the bare particle volume. With this choice of the cube size, an average of $\kappa_{agg} = 15.7\%$ is found from this geometrical description.

In order to check the general validity of our approach, it has then been applied to a series of more or less dense aggregates generated with different algorithms as outlined in the ESI. Contrarily to the aggregate shown in Fig. 7a, where any number of spheres can touch a given sphere as long as excluded volume is respected, new ensembles of aggregates have been created by varying the allowed number of direct neighbors in the simulation reaching different compacities. Three examples of such aggregates are shown in Fig. 8a, together with the structure factors that have been calculated as averages over hundreds of aggregates. The correlation hole is found to deepen as the geometrically determined compacity κ_{agg} increases from ca. 18 to 22%. In parallel, the real-space images show that aggregates become less fuzzy and denser, which is also seen in reciprocal space, as the first maximum of the form factor oscillation of spherical aggregate shapes shows up around 0.007 $Å^{-1}$. As a result, the compacity κ of these aggregates extracted using eqns (5) and (8) evolves from 15.3% to 25.7%.

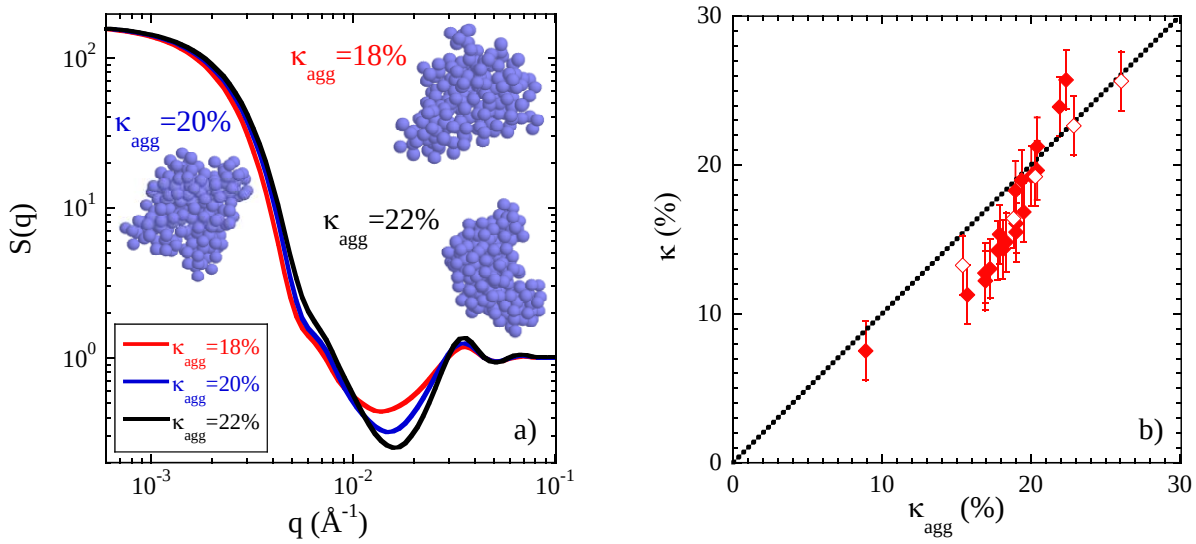

Fig. 8 (a) Evolution of S(q) of aggregates (N_{agg} = 200, same spheres R_0 = 10 nm, σ = 15%) of various compacities. Snapshots are shown in the insets. **(b)** Comparison of geometrically determined local density κ_{agg} to κ deduced from correlation hole analysis. Plain symbols: different construction algorithms with N_{agg} = 200, empty symbols: N_{agg} varying from 50 to 800 for a fixed algorithm (see details in ESI).

The comparison between the compacities determined with the geometrical approach in real space based on cubes (κ_{agg}, Fig. 7b), and the one obtained from the correlation hole analysis (κ) is shown in Fig. 8b, for all aggregates generated for this study using the algorithms given in the ESI. This comparison validates our approach: it means that a local density, on the scale of the first coordination shell, is successfully estimated by the correlation hole of the structure factor. We have also extended our calculations to aggregates of different sizes (N_{agg} = 50 to 800, see ESI), and the results convincingly join the data points on Fig. 8b.

The work by Beaucage and in particular the unified scattering law [27, 30] may be used to benchmark the predictions of our model as shown in Figure 8b. The particle density using, e.g., a two-level Beaucage fit can be determined using the ratio of prefactors (giving the aggregation number) together with the radius of gyration or of the equivalent sphere of the upper level. This approach needs more care in presence of particle polydipersity, which changes the ratio of the prefactors. By construction, this method gives the average density, as the radius of gyration does not account for the local density. In a semi-empirical approach,[31, 32] Beaucage proposes to take correlations into account, with two parameters, a correlation length and a local density. In the ESI, we have applied a two-level model with and without correlations to our data in Figure 7a. While the purely fractal law does not describe the correlation hole, the correlation term with a local density of 15% approaches the experimental curve somewhat in the intermediate q-range. Note that alternative choices of up to 25% are possible.

We thus conclude that our method is compatible with the semi-empirical approach by Beaucage, and possibly more precise.

The comparisons shown in Fig. 8b indicate that our approach is robust for aggregates of different internal structure. Moreover, we have checked that different aggregate masses correspond to aggregates of different structure, each characterized by a different κ. One should not, however, claim exaggerated precision. From all the examples given in this article, an error bar of ±15% on κ seems acceptable. Last but not least, it is recalled that κ is an average quantity characterizing local interactions, not suitable for, e.g., describing the global density, e.g. of very big fractal aggregates, for which it decreases strongly with size. Along the same lines, too small and too 'linear' aggregates are probably not suited for the present analysis. One should also keep in mind that distributions of aggregation numbers, in particular coexistence of isolated nanoparticles, will be described by an average compacity. Averaging is based on the convex shape of eqn (5) and thus introduces a peculiar weighting, underestimating κ. In any event, the exact value of the local density depends on the scale of observation, due to the intrinsically heterogeneous nature of aggregates. We have shown, however, that a trustworthy and useful estimate can be obtained easily from the scattered intensity.

5. Conclusion

We have shown in this article that the local volume fraction κ of spherical nanoparticles in dense assemblies or aggregates can be extracted in a robust and straightforward manner from a minimum – the correlation hole – in the experimentally observed small-angle scattering function, if the particle form factor is known. The simulations have been performed for "infinite" systems of known density first, with parameters given by eqn (7) already providing an acceptable estimate of κ. As finite systems are closer to the application of aggregates, the mapping procedure was further improved with finite subsets of the same density. The main result given by eqns (5) and (8) works in presence of polydispersity, and at any concentration of aggregates, because it is not based on the low-q intensities, but on a particular experimentally determined wave vector q_0. In spite of its simplicity, our method has been shown to deliver trustworthy estimates even in the unfavorable (but common) case where the exact nature of the interactions between NPs is unclear, due to the dominant HS interactions, in particular at higher local densities.

We emphasize that the present simulations have been performed with log-normally distributed polydisperse hard spheres. Real particles may differ, with two consequences: first, due to adsorbed or grafted layers, or intrinsic non-uniform scattering densities, non-spherical shapes, or non log-normal distribution functions, the average scattering of the individual particles may be different. This would result in a different form factor, but as long as particles can be well described as spherically symmetric, the experimental form factor can still be used to extract the apparent structure factor

described in this article. On the other hand, the interactions between particles will not be correctly described for strongly facetted NPs, violently polydisperse size distributions like strong bidispersity, or too thick adsorbed polymer layers with interactions impeding hard sphere repulsion. In practice, aggregates must be large enough that it makes sense to speak about their internal structure (typically $N_{agg} > 100$, see Figure 5b), and then the local density has been shown to be correctly determined between about 5 to 30%. The lower limit is probably a few percent given by the necessity of connectivity between particles, while we expect the upper limit to be even higher.

For the sake of completeness, it is noted that (possibly more involved) reverse Monte Carlo simulations of NP assemblies may give direct 3D information [61]. The advantage of such simulations is that they may describe entire intensity curves, and propose possible structures and correlation functions of 3D assemblies. However, they usually require additional knowledge like total aggregate masses, either from scattering down to low enough angles, or from other sources like microscopy. Moreover, depending on density, such techniques may require simulations of very big systems and thus be time-demanding, whereas the mapping proposed here is a straightforward application of eqns (5,8). The same is true with alternative integral equation modeling, which furthermore necessitates knowledge of interaction potentials.

There are applications of the present mapping procedure to about any assembly made of nanoparticles, in any matrix, even micellar aggregates [62-64] or mineral particles [65] in water, with attractive interactions mediated by polymer chains. In experimental studies of colloidal gels, the correlation hole was found to be well-defined and unchanged during the gelation process, and could be used to describe the average local particle density. [66] Simulations of attractive particles provide a representative application of our mapping procedure. Del Gado et al. have investigated the structure of a colloidal gel at 5% nominal volume fraction. [67] Applying the infinite HS analysis (eqn (7)) to their high-temperature fluid structure factor leads to an average density of about 4%. At low temperature, the structure evolves towards a gel with a low-q upturn and a correlation hole, describable by a finite sub-set (eqn (8)). In this case, the local volume fraction is obtained to be 7%, illustrating the local densification due to sticky interactions. The correlation hole analysis appears thus to be a simple and suitable tool. Moreover, it can also be used to quantify tendencies of κ along variations of experimental or simulation parameters. Our personal perspective is to use it for the analysis of local NP aggregates structure in polymer nanocomposites, as applied by us previously on industrial [22] and model systems [18, 68], however without detailed knowledge of the background and limits of the mapping procedure. In this context, high filler concentrations are usually of industrial interest, and our method works regardless of interactions between aggregates, as we focus on internal aggregate structure characterized by intermediate-q scattering.

Acknowledgements: The authors are thankful for support by the ANR NANODYN project, grant ANR-14-CE22-0001-01 of the French Agence Nationale de la Recherche. J.S. Pedersen (Aarhus) and L. Belloni (Saclay) are warmly thanked for illuminating discussions: in particular, the former for reminding us of the properties of eqn (1), and the second for providing us with a numerical tool implementing a solution of OZ integral equations, allowing the cross check of our results in Fig. 1b. Critical reading and suggestions by L. Cipelletti and W. Kob on a preliminary version are gratefully acknowledged.

References

1 D. Wang, B. Tejerina, I. Lagzi, B. Kowalczyk and B. A. Grzybowski, *ACS Nano*, 2011, **5**, 530-536.

2 J. Jancar, J. F. Douglas, F. W. Starr, S. K. Kumar, P. Cassagnau, A. J. Lesser, S. S. Sternstein and M. J. Buehler, *Polymer*, 2010, **51**, 3321-3343.

3 G. Schmidt and M. M. Malwitz, *Curr. Opin. Colloid Interface Sci*, 2003, **8**, 103-108.

4 O. Spalla, S. Lyonnard and F. Testard, *J. Appl. Cryst*, 2003, **36**, 338-347.

5 G. Heinrich, M. Kluppel and T. A. Vilgis, *Curr. Opin. Solid State Mater. Sci*, 2002, **6**, 195-203.

6 D. Wen, W. Liu, D. Haubold, C. Zhu, M. Oschatz, M. Holzschuh, A. Wolf, F. Simon, S. Kaskel and A. Eychmüller, *ACS Nano*, 2016, **10**, 2559-2567.

7 G. P. Baeza, J. Oberdisse, A. Alegria, M. Couty and A. C. Genix, *Phys. Chem. Chem. Phys.*, 2015, **17**, 1660-1666.

8 M. Klüppel, in *Filler-Reinforced Elastomers/Sanning Force Microscopy*, eds. B. Capella, M. Geuss, M. Klüppel, M. Munz, E. Schulz and H. Sturm, Springer Berlin Heidelberg, Berlin, Heidelberg, 2003, pp. 1-86.

9 S. T. Jones, Z. Walsh-Korb, S. J. Barrow, S. L. Henderson, J. del Barrio and O. A. Scherman, *ACS Nano*, 2016, **10**, 3158-3165.

10 S. A. Hassan, *ACS Nano*, 2017, **11**, 4145-4154.

11 M. Yue, Y. Li, Y. Hou, W. Cao, J. Zhu, J. Han, Z. Lu and M. Yang, *ACS Nano*, 2015, **9**, 5807-5817.

12 S. K. Kumar, N. Jouault, B. Benicewicz and T. Neely, *Macromolecules*, 2013, **46**, 3199-3214.

13 D. Le Strat, F. Dalmas, S. Randriamahefa, J. Jestin and V. Wintgens, *Polymer*, 2013, **54**, 1466–1479.

14 A. P. Holt, V. Bocharova, S. Cheng, A. M. Kisliuk, B. T. White, T. Saito, D. Uhrig, J. P. Mahalik, R. Kumar, A. E. Imel, T. Etampawala, H. Martin, N. Sikes, B. G. Sumpter, M. D. Dadmun and A. P. Sokolov, *ACS Nano*, 2016, **10**, 6843-6852.

15 G. P. Baeza, C. Dessi, S. Costanzo, D. Zhao, S. Gong, A. Alegria, R. H. Colby, M. Rubinstein, D. Vlassopoulos and S. K. Kumar, *Nat. Commun.*, 2016, **7**, 11368.

16 S. Cheng, S.-J. Xie, J.-M. Y. Carrillo, B. Carroll, H. Martin, P.-F. Cao, M. D. Dadmun, B. G. Sumpter, V. N. Novikov, K. S. Schweizer and A. P. Sokolov, *ACS Nano*, 2017, **11**, 752-759.

17 G. P. Baeza, A. C. Genix, C. Degrandcourt, L. Petitjean, J. Gummel, R. Schweins, M. Couty and J. Oberdisse, *Macromolecules*, 2013, **46**, 6388–6394.

18 A. Banc, A. C. Genix, M. Chirat, C. Dupas, S. Caillol, M. Sztucki and J. Oberdisse, *Macromolecules*, 2014, **47**, 3219–3230.

19 A.-C. Genix and J. Oberdisse, *Curr. Opin. Colloid Interface Sci*, 2015, **20**, 293-303.

20 C. Chevigny, F. Dalmas, E. Di Cola, D. Gigmes, D. Bertin, F. Boué and J. Jestin, *Macromolecules*, 2011, **44**, 122-133.

21 F. Dalmas, N. Genevaz, M. Roth, J. Jestin and E. Leroy, *Macromolecules*, 2014, **47**, 2044-2051.

22 G. P. Baeza, A. C. Genix, C. Degrandcourt, L. Petitjean, J. Gummel, M. Couty and J. Oberdisse, *Macromolecules*, 2013, **46**, 317-329.

23 C. Schmitt Pauly, A.-C. Genix, J. G. Alauzun, J. Jestin, M. Sztucki, P. H. Mutin and J. Oberdisse, *Polymer*, 2016, **97**, 138-146.

24 O. Pravaz, B. Droz, P. Schurtenberger and H. Dietsch, *Nanoscale*, 2012, **4**, 6856-6862.

25 J. S. Meth, S. G. Zane, C. Chi, J. D. Londono, B. A. Wood, P. Cotts, M. Keating, W. Guise and S. Weigand, *Macromolecules*, 2011, **44**, 8301-8313.

26 J. Teixeira, *J Appl Crystallogr*, 1988, **21**, 781-785.

27 G. Beaucage, *J Appl Crystallogr*, 1995, **28**, 717-728.

28 J. K. Kjems, T. Freltoft, D. Richter and S. K. Sinha, *Physica B+C*, 1986, **136**, 285-290.

29 S. K. Sinha, *Physica D: Nonlinear Phenomena*, 1989, **38**, 310-314.

30 G. Beaucage, H. K. Kammler and S. E. Pratsinis, *Journal of Applied Crystallography*, 2004, **37**, 523-535.

31 G. Beaucage, T. A. Ulibarri, E. P. Black and D. W. Schaefer, in *Hybrid Organic-Inorganic Composites*, American Chemical Society, 1995, vol. 585, ch. 9, pp. 97-111.

32 G. Beaucage, in *Polymer Science: A Comprehensive Reference*, ed. M. a. Möller, Elsevier BV, Amsterdam, 2012, vol. 2, pp. 399–409.

33 J. I. Langford and A. J. C. Wilson, *J. Appl. Cryst*, 1978, **11**, 102-113.

34 M. Fasolo and P. Sollich, *Phys. Rev. Lett*, 2003, **91**, 068301.

35 N. Lutterbach, H. Versmold, V. Reus, L. Belloni and T. Zemb, *Langmuir*, 1999, **15**, 337-344.

36 N. Lutterbach, H. Versmold, V. Reus, L. Belloni, T. Zemb and P. Lindner, *Langmuir*, 1999, **15**, 345-352.

37 B. D'Aguanno and R. Klein, *J. Chem. Soc. Faraday Trans.*, 1991, **87**, 379-390.

38 K. Mortensen, W. Brown, K. Almdal, E. Alami and A. Jada, *Langmuir*, 1997, **13**, 3635-3645.

39 K. Hiroike, *J. Phys. Soc. Jpn.*, 1969, **27**, 1415-&.

40 K. Hiroike and Y. Fukui, *Progr. Theor. Exp. Phys.*, 1970, **43**, 660-671.

41 L. Blum and G. Stell, *J. Chem. Phys.*, 1979, **71**, 42-46.

42 D. Gazzillo and A. Giacometti, *J. Chem. Phys.*, 2000, **113**, 9837-9848.

43 D. Gazzillo and A. Giacometti, *J. Chem. Phys.*, 2004, **120**, 4742-4754.

44 A. Vrij, *J. Chem. Phys.*, 1978, **69**, 1742-1747.

45 A. Vrij, *J. Chem. Phys.*, 1979, **71**, 3267-3270.

46 A. Vrij, *J. Colloid Interface Sci.*, 1982, **90**, 110-116.

47 D. Musino, A.-C. Genix, C. Fayolle, A. Papon, L. Guy, N. Meissner, R. Kozak, P. Weda, T. Bizien, T. Chaussée and J. Oberdisse, *Macromolecules*, 2017, **50**, 5138–5145.

48 A.-C. Genix, C. Schmitt-Pauly, J. G. Alauzun, T. Bizien, P. H. Mutin and J. Oberdisse, *Macromolecules*, 2017.

49 G. Despert and J. Oberdisse, *Langmuir*, 2003, **19**, 7604-7610.

50 R. J. Baxter, *J. Chem. Phys.*, 1968, **49**, 2770-2774.

51 D. Frenkel, R. J. Vos, C. G. d. Kruif and A. Vrij, *J. Chem. Phys.*, 1986, **84**, 4625-4630.

52 J. S. Pedersen, in *Neutrons, X-ray and Light Scattering*, eds. P. Lindner and T. Zemb, Elsevier, North Holland, 2002, ch. 15, p. 381.

53 J. S. Pedersen and P. Schurtenberger, *Europhys. Lett.*, 1999, **45**, 666.

54 L. Cannavacciuolo, C. Sommer, J. S. Pedersen and P. Schurtenberger, *Phys. Rev. E*, 2000, **62**, 5409-5419.

55 L. Cannavacciuolo, J. S. Pedersen and P. Schurtenberger, *Langmuir*, 2002, **18**, 2922-2932.

56 P. Debye, *Ann. Phys. (Berlin)*, 1915, **46**, 809-823.

57 J. K. Percus and G. J. Yevick, *Phys Rev*, 1958, **110**, 1-13.

58 N. W. Ashcroft and D. C. Langreth, *Phys Rev*, 1967, **156**, 685-692.

59 J. P. Hansen and I. R. McDonald, *Theory of Simple Liquids*, Academic Press, London, 1986.

60 N. F. Carnahan and K. E. Starling, *J. Chem. Phys.*, 1969, **51**, 635-636.

61 J. Oberdisse, P. Hine and W. Pyckhout-Hintzen, *Soft Matter*, 2007, **2**, 476-485.

62 P. Herve, M. Destarac, J. F. Berret, J. Lal, J. Oberdisse and I. Grillo, *Europhys. Lett.*, 2002, **58**, 912-918.

63 J. F. Berret, P. Herve, O. Aguerre-Chariol and J. Oberdisse, *J. Phys. Chem. B*, 2003, **107**, 8111-8118.

64 J. F. Berret, G. Cristobal, P. Herve, J. Oberdisse and I. Grillo, *Eur Phys J E*, 2002, **9**, 301-311.

65 K. Yokota, M. Morvan, J. F. Berret and J. Oberdisse, *Europhys. Lett.*, 2005, **69**, 284-290.

66 P. J. Lu, E. Zaccarelli, F. Ciulla, A. B. Schofield, F. Sciortino and D. A. Weitz, *Nature*, 2008, **453**, 499-503.

67 E. D. Gado and W. Kob, *Europhys. Lett.*, 2005, **72**, 1032.

68 M. Tatou, A. C. Genix, A. Imaz, J. Forcada, A. Banc, R. Schweins, I. Grillo and J. Oberdisse, *Macromolecules*, 2011, **44**, 9029-9039.